

José M. Seguí-Simarro · L. Andrew Staehelin

Cell cycle-dependent changes in Golgi stacks, vacuoles, clathrin-coated vesicles and multivesicular bodies in meristematic cells of *Arabidopsis thaliana*: A quantitative and spatial analysis

Received: 16 February 2005 / Accepted: 11 July 2005 / Published online: 3 September 2005
© Springer-Verlag 2005

Abstract Cytokinesis in plants involves both the formation of a new wall and the partitioning of organelles between the daughter cells. To characterize the cellular changes that accompany the latter process, we have quantitatively analyzed the cell cycle-dependent changes in cell architecture of shoot apical meristem cells of *Arabidopsis thaliana*. For this analysis, the cells were preserved by high-pressure freezing and freeze-substitution techniques, and their Golgi stacks, multivesicular bodies, vacuoles and clathrin-coated vesicles (CCVs) characterized by means of serial thin section reconstructions, stereology and electron tomography techniques. Interphase cells possess ~35 Golgi stacks, and this number doubles during G2 immediately prior to mitosis. At the onset of cytokinesis, the stacks concentrate around the periphery of the growing cell plate, but do not orient towards the cell plate. Interphase cells contain ~18 multivesicular bodies, most of which are located close to a Golgi stack. During late cytokinesis, the appearance of a second group of cell plate-associated multivesicular bodies coincides with the onset of CCV formation at the cell plate. During this period a 4× increase in CCVs is paralleled by a doubling in number and a 4× increase in multivesicular bodies volume. The vacuole system also undergoes major changes in organization, size, and volume, with the most notable change seen during early telophase cytokinesis. In particular, the vacuoles form sausage-like tubular compartments with a 50% reduced surface area and an 80% reduced

volume compared to prometaphase cells. We postulate that this transient reduction in vacuole volume during early telophase provides a means for increasing the volume of the cytosol to accommodate the forming phragmoplast microtubule array and associated cell plate-forming structures.

Keywords Clathrin-coated vesicles · Electron tomography · Golgi · Multivesicular bodies · Stereology (shoot meristem cells) · *Arabidopsis*

Abbreviations CCV: Clathrin-coated vesicle · dn: Mean nuclear diameter · Dn: Corrected mean nuclear diameter · EM: Electron microscopy · ER: Endoplasmic reticulum · MVB: Multivesicular body · Na: Plane numerical density · Nv: Numerical density · Sv: Surface density · TGN: Trans-Golgi network · Vv: Volume density

Introduction

Cytokinesis, the partitioning of the daughter cytoplasm after mitosis, is the final event of cell division. In plants, this partitioning involves the formation of a cell plate that is transformed into a new cell wall. The structural events associated with the formation of the cell plate during somatic type cytokinesis have been recently described in considerable detail by means of electron tomography of cryofixed and freeze-substituted cells (Seguí-Simarro et al. 2004). The involvement of membranous organelles, like the endoplasmic reticulum (ER) both in mitosis and cytokinesis has been extensively studied in the past decades (Hepler and Wolniak 1984; Baskin and Cande 1990; Seguí-Simarro et al. 2004). In contrast, only sketchy information is available on the cell cycle-dependent changes in other organelles that also participate in the processes of cell plate assembly and maturation, the Golgi apparatus, multivesicular bodies (MVBs) and vacuoles.

J. M. Seguí-Simarro (✉) · L. A. Staehelin
Department of Molecular, Cellular and Developmental Biology,
University of Colorado, UCB 347, Boulder, CO 80309-0347, USA

Present address: J. M. Seguí-Simarro
Centro de Conservación y Mejora de la Agrodiversidad Valenciana
(COMAV), Universidad Politécnica de Valencia, Camino de Vera,
s/n, edificio 9B, 46022, Valencia, Spain
E-mail: seguisim@btc.upv.es
Tel.: +34-96-3877000
Fax: +34-96-3879422

The Golgi apparatus of plant cells is a carbohydrate assembling and processing organelle that consists of many individual Golgi stack units (Hawes and Brandizzi 2004). During interphase, the Golgi stacks are dispersed (Hepler and Wolniak 1984) and undergo myosin-dependent stop-and-go movements along actin filaments that are anchored to ER membranes (Nebenführ et al. 1999; Nebenführ and Staehelin 2001). It was previously thought that throughout mitosis, the plant Golgi stacks do not organize in any particular region (Hepler and Wolniak 1984), but recently, Nebenführ et al. (2000) showed that when cultured tobacco BY-2 cells enter mitosis, the rapid saltatory movements of the Golgi stacks cease, and a subset of stacks redistribute, first around the mitotic spindle and then around the phragmoplast, giving rise to a “Golgi belt” in the equatorial plane. This redistribution reflects the redirection of the default secretory pathway from the plasma membrane to the cell plate (Batoko et al. 2000; Jürgens 2004). Another discrepancy revolves around the timing of Golgi stack division. Based on a stereological analysis of onion root meristem cells, the cell cycle-dependent doubling of Golgi stacks has been suggested to occur during mitosis (Garcia-Herdugo et al. 1988), whereas another study of cultured *Catharanthus roseus* cells has led to the suggestion that they divide during cytokinesis (Hirose and Komamine 1989).

Multivesicular bodies, also known as “multivesicular endosomes” in the mammalian and yeast cell literature (Marcote et al. 2000), are small spherical organelles with internal vesicles. Their principal function is to serve as intermediate protein sorting and processing compartments between the *trans*-Golgi network (TGN) and either lytic vacuoles (lysosomes) or storage vacuoles (Jürgens 2004). In plants, the association of MVBs with the endocytic pathway was initially deduced from endocytic tracer uptake studies with protoplasts (Tanchak and Fowke 1987), but until recently, little else was known about their function. A recent study involving tobacco BY-2 cells, has demonstrated that MVBs serve as prevacuolar compartments (Tse et al. 2004). Budding, clathrin-coated vesicles are a characteristic feature of maturing cell plates, and their appearance coincides with the formation of the first cell plate-associated MVBs (Samuels et al. 1995; Otegui et al. 2001; Seguí-Simarro et al. 2004). It has been postulated that these clathrin-coated vesicles remove selected membrane components and excess membrane from the maturing cell plates and then shunt them to MVBs for recycling or degradation.

Plant vacuoles are highly dynamic and versatile organelles that vary greatly in size, shape and function (Staehelin and Newcomb 2000). Vacuoles can be functionally divided into two types: storage and lytic (Marty 1999; Jürgens 2004). The lytic vacuoles of plants are functionally equivalent to animal lysosomes and yeast vacuoles. They serve as the last compartment in the endocytic pathway, where cellular waste is degraded and stored (Jürgens 2004). Mature MVBs appear to fuse with these vacuoles (Marty 1999). The best studied

storage vacuoles of plants, the protein storage vacuoles, are mostly found in developing seeds (Herman and Larkins 1999). Although the variable shape of plant vacuoles is well known, little specific information is available on the cell cycle-dependent changes in vacuolar architecture in meristem cells. In horseradish root meristems, provacuolar tubular clusters have been reported to exhibit a polarized organization during mitosis (Marty 1999). In cultured tobacco BY-2 cells, vacuolar tubules surround the mitotic spindle, and interact with the phragmoplast during cytokinesis (Kutsuna and Hasezawa 2002; Kutsuna et al. 2003).

To gain a better understanding of the roles of these organelles in plant cytokinesis, we have investigated how their architecture and spatial organization change during the cell cycle in apical meristem cells of *Arabidopsis*. In particular, we have employed 3D reconstructions of carefully staged, cryofixed and serial sectioned whole cells, and tomographic reconstructions of serial thick sections to obtain information on changes in shape, number, volume, and distribution of Golgi stacks, clathrin-coated vesicles, MVBs, and vacuoles during the cell cycle. These techniques provide accurate information on morphological, numerical and distributional changes of the studied organelles. To assess the statistical validity of the numerical data, we also applied electron microscopy (EM) stereology methods that confirmed the findings observed in single cell reconstructions.

Materials and methods

Plant material

Seeds of *Arabidopsis thaliana* L. (Landsberg *erecta* wild type; Lehle seeds, Texas, OR) were planted in 0.8% (w/v) agar plates with MS for 2 days and then acclimated over a period of 3 days with increasing sucrose concentrations as follows: 50 mM sucrose for 48 h and 100 mM sucrose for 24 h prior to cryofixation. Seedlings were grown at a temperature of 24°C and a 16 h photoperiod.

High-pressure freezing and freeze-substitution

Shoot apical meristems and leaf primordia were excised from 5-day-old seedlings, transferred to aluminum sample holders, cryoprotected with 150 mM sucrose, and frozen in a Baltec HPM 010 high-pressure freezer (Technotrade, Manchester, NH), and then transferred to liquid nitrogen. The samples were then freeze-substituted in 4% OsO₄ in anhydrous acetone at –80°C for 5 days, warmed to room temperature, infiltrated with Epon resin (Ted Pella, Inc., Redding, CA) and polymerized according to Seguí-Simarro et al. (2004). The resulting plastic-embedded tissue blocks were then used to obtain 100 nm sections for stereology, serial section

reconstruction and 300 nm sections for electron tomography.

Electron microscopy and serial section reconstruction

Ribbons of serial sections were collected, mounted on grids, and stained as described (Seguí-Simarro et al. 2004). Interphase cells at different stages (G1, S and G2) were selected from the sections according to the following morphological criteria: nuclear/cytoplasmic surface area ratio, which progressively decreases from G1 to G2 (Seguí-Simarro 2001); nuclear size, which increases at the S phase; nucleolar architecture, which exhibits different changes in their main components (dense fibrillar component, fibrillar centers, granular component and nucleolar vacuoles) as the cell progresses through the cell cycle (Risueño and Medina 1986; Risueño et al. 1988; Seguí-Simarro 2001); and cell wall thickness, which progressively increases after the new cell wall is formed (Seguí-Simarro 2001). As a reference of a mitotic stage prior to cytokinesis, a prometaphase cell was also selected. This stage was determined by the presence of a discontinuous nuclear envelope within which the condensed chromosomes begin to arrange. The cytokinetic stages (solid and ring phragmoplast) were selected according to the differential architecture that the developing cell plate presents at these stages (Seguí-Simarro et al. 2004). Single digital micrographs of at least 15 different cells were taken and analyzed for both distributional and quantitative changes. For whole cell serial section reconstructions, digital micrographs were converted into stacks of serial images and aligned with the 3dmod software package (Kremer et al. 1996). To adjust the reconstructions to the actual cell volume, a correction factor was applied only to the Z-axis, calculated by dividing the section thickness by the pixel size in the digital micrographs.

Stereological methods

For stereology, we analyzed single digital electron micrographs from 41 meristematic dividing and 29 interphase cells, determined by the presence of condensed chromosomes or interphase nucleus, respectively. Cells were arbitrarily chosen from sections of shoot apical meristems and leaf primordia of nine different plantlets and arbitrarily selected from three different processing batches. The minimum number of micrographs was determined using the progressive mean test (de Paz 1998), with a minimum confidence limit of $\alpha=0.05$. It is based on the progressive increase of the sample size with new micrograph data, and the comparison of the new mean and standard deviation (SD) with the previous ones. The minimum representative sample size is the point after which the new mean and SD do not deviate more than 5% from the previous

mean and SD, irrespective of the number of new micrographs added.

For the calculation of cell volumes, pictures comprising several cells were taken at a constant magnification (3400 \times). Morphometric measurements were obtained with the UTHSCS1A Image Tool program (<http://ddsdx.uthscsa.edu/dig/itdesc.html>). In interphase cells, the micrograph, cell and nuclear area as well as perimeter were measured for each micrograph. Then, using these values we calculated, for both cell vs micrograph (c-m) and nucleus vs cell (n-c), the following basic stereological parameters (Williams 1977; de Paz 1998): plane numerical density (Na), surface density (Sv), volume density (Vv) and numerical density (Nv). The mean nuclear diameter (dn) was also calculated from the averaged nuclear perimeter, and then the corrected mean diameter (Dn) was deduced from the formula $Dn = 4dn/\pi$ (Williams 1977; de Paz 1998). With Dn, we calculated the nuclear volume (Vn) according to the geometrical formula for the volume of a sphere $Vn = (4/3)\pi(Dn/2)^3$. The cellular volume (Vc) was calculated as $Vc = Vn/Vv_{n-c}$ according to Williams (1977). Since dividing (mitotic) cells showed no nucleus, the Vc in dividing cells was estimated from the ratios between Vv_{c-m} in interphase and dividing cells as follows: $Vc_{dividing} = (Vv_{c-m,dividing} / Vv_{c-m,interphase}) \cdot Vc_{interphase}$.

For the calculation of the number of Golgi stacks and MVBs in interphase and dividing cells, pictures covering the whole cell were taken at a constant magnification of 7900 \times . For both interphase and dividing cells, the area of the cell, Golgi stacks and MVBs was measured, as well as the number of stacks and MVBs per cell, calculating with them Na and Vv for each stack or MVB with respect to the cell ($s-c$). Na and Vv were averaged and then used to calculate Nv_{s-c} , using the formula $Nv_{s-c} = (1/\beta)(Na_{s-c}^{3/2} / Vv_{s-c}^{1/2})$, (Steer 1981), where $\beta=1.72$ for the Golgi stacks, according to the corresponding value deduced by Garcia-Herdugo et al. (1988) for plant Golgi stacks. For the MVBs we assumed spherical shape, using the β value corresponding to the spheres (1.38). Finally, the number of stacks and MVBs per cell was deduced by multiplying Nv_{s-c} by the previously deduced cell volume.

Standard deviations were calculated by Taylor series expansions of multivariate functions (Hahn and Shapiro 1967). For all calculations of Nv, a confidence interval was estimated using a first-order Taylor expansion of the Nv equation around the mean Na and Nv values. The size of the confidence interval calculated this way never deviated by more than 25% from the calculated Nv value.

To estimate the ratio of vacuolar vs cell volume, we measured the vacuolar and total cell area of the pictures covering the six considered cell cycle stages (see above). According to the Delesse principle (Delesse 1847), these areas are estimators of the corresponding volumes. The ratio was obtained by dividing the vacuolar area by the total area.

Intermediate/high-voltage electron microscopy and 3D tomographic reconstruction

Epon (300 nm thick) sections of dividing cells were collected and processed as described (Seguí-Simarro et al. 2004). A FEI Tecnai TF30 intermediate voltage electron microscope (FEI, Hillsboro, OR, USA) operating at 300 kV, and a JEM-1000 high-voltage electron microscope (JEOL, Akishima, Tokyo, Japan) operating at 750 kV, were used to collect tilt series of images about two orthogonal axes, according to (Mastronarde 1997). The series were aligned and the tomographic volumes reconstructed as described (Mastronarde 1997; Otegui et al. 2001; Seguí-Simarro et al. 2004).

Modeling and three-dimensional analysis

Tomograms and serial section reconstructions were displayed, modeled and analyzed with the 3dmod software package (formerly imod; (Kremer et al. 1996) as described (Otegui et al. 2001; Seguí-Simarro et al. 2004). For the serial section reconstructions, the Golgi stacks with their corresponding TGNs, the MVBs, the nucleus/chromosomes, and the plasma membrane/cell plate were modeled. Total volumes and surface areas of organelles were calculated with the imodinfo program. For the tomograms, the cell plate and the clathrin-coated vesicles (CCVs) were modeled. The density of CCVs around the cell plate was calculated dividing their number by the tomographic volume within a distance of 500 nm around the cell plate.

Results

We have employed three complementary structural techniques to characterize in both qualitative and quantitative terms the cell cycle-dependent changes in the organization of Golgi stacks (Fig. 1, 2, 3), MVBs (Fig. 4, 5), CCVs (Fig. 2, 5) and vacuoles (Fig. 6, 7) in apical meristem cells of *Arabidopsis*. The three techniques are stereology of random thin EM sections, serial thin section analysis of entire cells, and electron tomography. The stereology studies yielded statistically representative estimations of numbers of Golgi stacks (Table 1), as well as numbers and volumes of multivesicular bodies (Fig. 5). The serial thin section reconstructions (~130–150 section images per cell; Imod software package; Kremer et al, 1996) produced insights into the spatial organization, numbers, surface areas and volumes of Golgi stacks (Fig. 3, Table 1), MVBs (Fig. 4) and vacuoles (Fig. 6, 7). The tomographic analyses, finally, provided information on the distribution and numbers of CCVs around maturing cell plates (Fig. 2, 5).

All the samples were preserved by high-pressure freezing and freeze-substitution techniques. The cell cy-

cle stage [G1, S, G2, prometaphase, early telophase (solid phragmoplast stage of cytokinesis) and late telophase (ring phragmoplast stage of cytokinesis)] for each cell analyzed in this study was determined by multiple morphological criteria such as nuclear/cytoplasmic surface area ratio, nuclear size and shape, nucleolar architecture, cell wall thickness, and presence and distribution of condensed chromosomes and/or a cell plate (see Materials and methods).

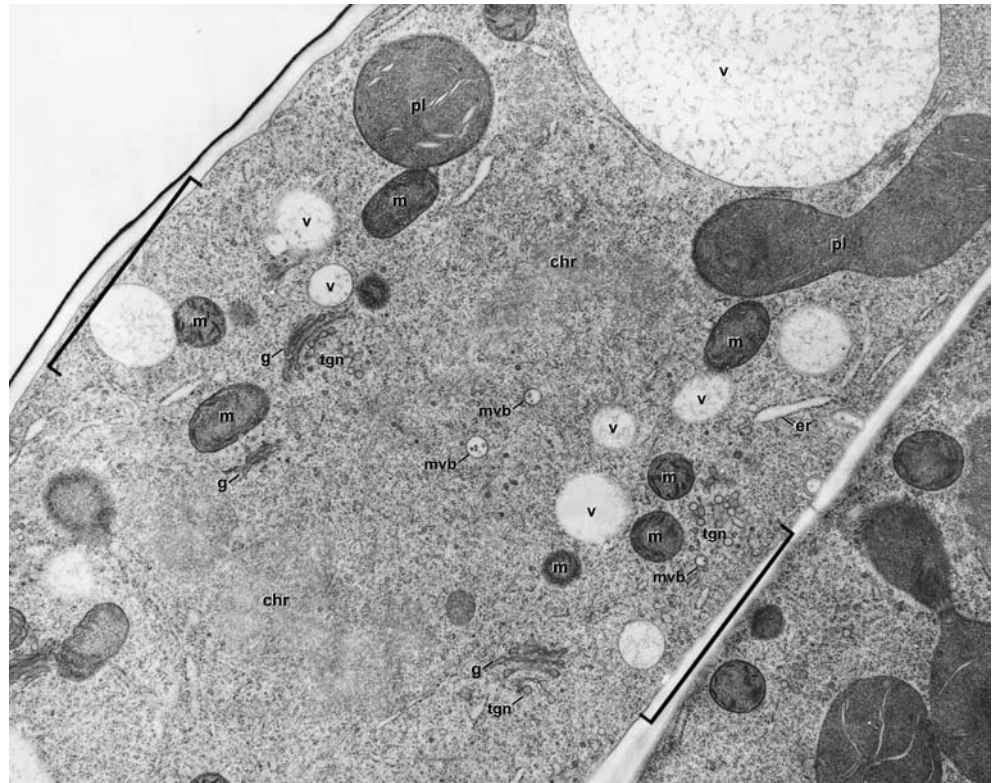
Golgi stacks double in number during G2, prior to mitosis

The stereological analysis showed that during interphase, the average apical meristem cell of *Arabidopsis* has a volume of ~204 μm^3 (nuclear volume ~43 μm^3 , 21%; cytoplasmic volume ~160 μm^3 , 79%). The numerical density N_v , defined as the density of Golgi stacks per volume unit, was 0.2 ± 0.05 , which implies ~36 Golgi stacks for the calculated cell volume (Table 1). Similar calculations for the dividing (mitotic and cytokinetic) cells yielded an average cell volume of ~379 μm^3 (1.8× the interphase cell volume). The N_v for Golgi stacks was 0.19 ± 0.04 , resulting in an average number of ~76 Golgi stacks per dividing cell (Table 1). These calculations proved that the number of Golgi stacks double as the cell volume increases during G2, prior to mitosis.

The Golgi stacks in *Arabidopsis* meristem cells are consistently composed of 4–6 cisternae and exhibit a distinct *cis-trans* structural polarity (Fig. 1, 2a, b; (Staelin et al. 1990). A distinct, bulbous TGN was also associated with the trans side of each Golgi stack (Fig. 1, 2a, b). However, no free-floating TGNs as observed in the yeast *Pichia pastoris* (Mogelsvang et al. 2003) or in maize root cap cells (Mollenhauer et al. 1991) were detected either in the serial section reconstructions or in the single electron micrographs.

The serial section reconstructions of three carefully staged interphase (G1, S, G2; Fig. 3a-c) and three carefully staged dividing cells (prometaphase; telophase: early and late cell plate formation; Fig. 3d-f) both confirmed and extended the stereological findings pertaining to the Golgi/trans-Golgi network (Golgi-TGN) complexes (Table 1). In the 3D models of the reconstructed cells shown in Fig. 3, the Golgi stacks are depicted as yellow, oriented cylinders with the position of the TGN marked by a red sphere. This mode of illustration provides a means for studying the distribution and orientation of the stacks throughout a cell as well as for determining their absolute number. In the G1 and S cells (Fig. 3a, b) we counted 34 and 36 Golgi stacks, respectively, whereas in the larger G2 cell, we found 66 stacks (Fig. 3c), and in the dividing cells (Fig. 3d-f) 69, 65, and 68 stacks, respectively. Interestingly, when the number of Golgi stacks were counted on either side of the developing cell plate (Fig. 3e,

Fig. 1 Electron micrograph of an *Arabidopsis* shoot meristem cell. Late anaphase cell at the phragmoplast initial stage of cytokinesis. Note the arrangement of Golgi stacks (g) and their trans-Golgi networks (tgn), multivesicular bodies (mvb), mitochondria (m), small and large vacuoles (v) and plastids (pl) surrounding the late mitotic-cytokinetic machinery (brackets). Bar: 1 μm



f), the distribution ratio was 55–45% between the future daughter cells. The increased size of the Golgi cylinders of the early telophase cell shown in Fig. 3e reflects an increase in diameter of the widest cisternae of the Golgi stacks.

Golgi stacks accumulate around, but do not reorient towards the cell plate during cytokinesis

Figure. 3 also illustrates the changes in spatial organization of the Golgi stacks throughout the cell cycle. During interphase, the Golgi stacks are seen to be randomly distributed throughout the cytoplasm even as the cells enlarge and the number of Golgi stacks increase (Fig. 3a–c). This arrangement persists during prometaphase (Fig. 3d), but then changes during early cytokinesis (early telophase; Fig. 3e), when cell plate growth reaches its maximal rate (Seguí-Simarro et al. 2004). During this stage of the cell cycle, most of the Golgi accumulate in a ring-like configuration, the Golgi belt (Nebenführ et al. 2000), around the forming cell plate (Fig. 3e insert). Of the 65 Golgi present in this cell, 54 (83%) were seen to be in close proximity to the cell plate. Lack of resolution in our serial thin section micrographs prevented us from modeling the phragmoplast microtubules. However, the presence of the Golgi-excluding phragmoplast microtubule array is evidenced by the absence of stacks from the cytoplasm adjacent to the growing plate regions, as seen in the face-on view of the cell plate and the Golgi belt depicted in the insert of Fig. 3e. The Golgi belt disappears during the final stages

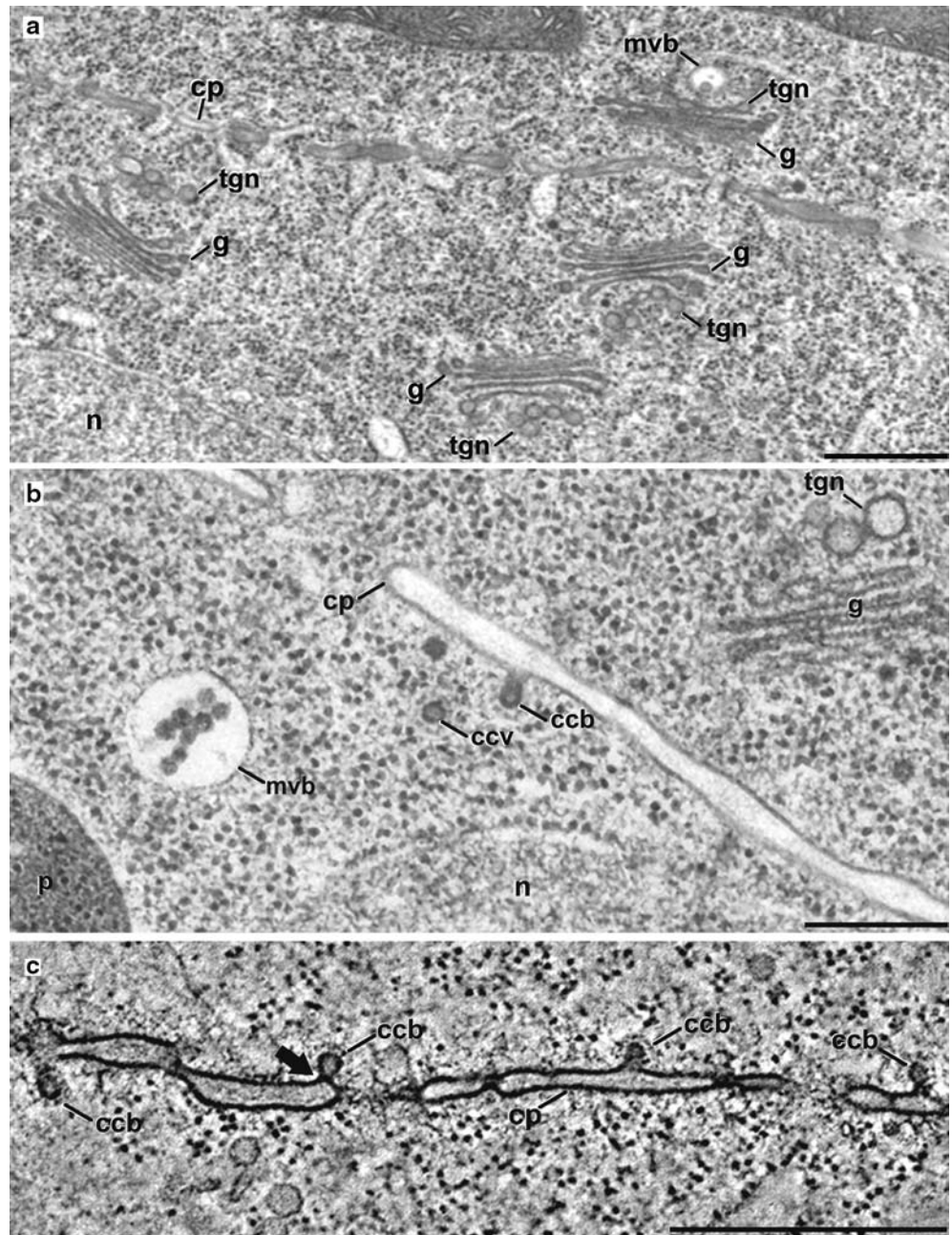
of cytokinesis and the Golgi re-assume a random distribution (Fig. 3f). Simultaneously, the two daughter nuclei move back closer to the cell plate.

It can be argued that the efficiency of vesicle trafficking from the Golgi–TGN system to the cell plate might be enhanced by orienting the Golgi–TGN complexes towards the forming cell plate region during cytokinesis. In random thin sections through cell plate-containing regions of dividing cells, the Golgi–TGN complexes appear to be randomly oriented, but a biased orientation cannot be excluded. To address this question in a more systematic manner, we have used our reconstructed dividing cell models to determine the percentage of Golgi stacks with the TGN oriented inwards, i.e., towards the mitotic spindle, phragmoplast or cell plate, vs those whose TGN was facing outwards, i.e., towards the cell wall. As a reference, we also measured the percentage of stacks oriented towards the nearest cell wall in interphase cells (G1, S, G2). In all the cells, the percentage of stacks oriented inward and outward was remarkably similar, never deviating more than 10% from an equal, 50:50%, distribution.

The majority of multivesicular bodies are seen in the vicinity of Golgi–TGN complexes and the cell plate

Multivesicular bodies, prevacuolar compartments containing vesicles, are commonly seen in meristem (Fig. 1, 2a, b) and in syncytial endosperm (Otegui et al. 2001) cells of *Arabidopsis*, as well as in dividing tobacco BY-2 cells (Samuels et al. 1995). In the apical meristem cells studied

Fig. 2 Electron micrographs and tomographic slice image of the cellular structures, except vacuoles, modeled in this study. **(a)** Fenestrated sheet-type cell plate (cp) of a mid telophase cell with Golgi stacks (g) and associated trans-Golgi network (tgn) cisternae. Note the random orientation of the Golgi stack-TGN units with respect to the cell plate, and the association of multivesicular bodies (mvb) with the TGN. **(b)** Fenestrated sheet-type cell plate (cp) with a clathrin-coated bud (ccb) and a free clathrin-coated vesicle (ccv). Clustered, dark vesicles are seen inside the multivesicular body (mvb). **(c)** Fenestrated sheet-type cell plate with multiple budding clathrin-coated vesicles (ccb). The arrow points to a dynamin-like ring around the neck of a clathrin-coated bud that is ready to be separated from the cell plate. g: Golgi stack. tgn: trans-Golgi network. n: nucleus. Bars: 500 nm



here, spherical or oval MVBs were seen during all stages of the cell cycle (Fig. 4), and their numbers were found to nearly double (~ 18 to ~ 40) between interphase and dividing cells, as estimated by stereology. Multivesicular bodies varied in size from 230 to 375 nm in diameter (Fig. 5a). During cell division in the reconstructed cells, we observed an increase in number from the onset of mitosis (prometaphase) to late telophase (late cytokinesis, ring phragmoplast stage; Fig. 5a). During these stages, the MVBs also reached their largest size, with the average volume increasing nearly fourfold between prometaphase and the ring phragmoplast stage of cytokinesis.

Multivesicular bodies were seen throughout all the cells, many of them appearing in clusters in the vicinity of TGN cisternae (Fig. 4a–d). The spatial relationship

between Golgi stacks and MVBs is most noticeable during the formation of the Golgi belt (early cell plate formation), where the increased concentration of Golgi stacks around the cell plate margins is paralleled by an increase in MVBs (Fig. 4e). During later stages of cytokinesis (Fig. 4f), a number of multivesicular bodies are also seen close to the forming cell plate.

A major increase in volume of MVBs during late stage cytokinesis is paralleled by a significant rise in the formation of cell plate-derived clathrin-coated vesicles

As evidenced in Fig. 4, MVBs often occur in small clusters, particularly those located adjacent to Golgi

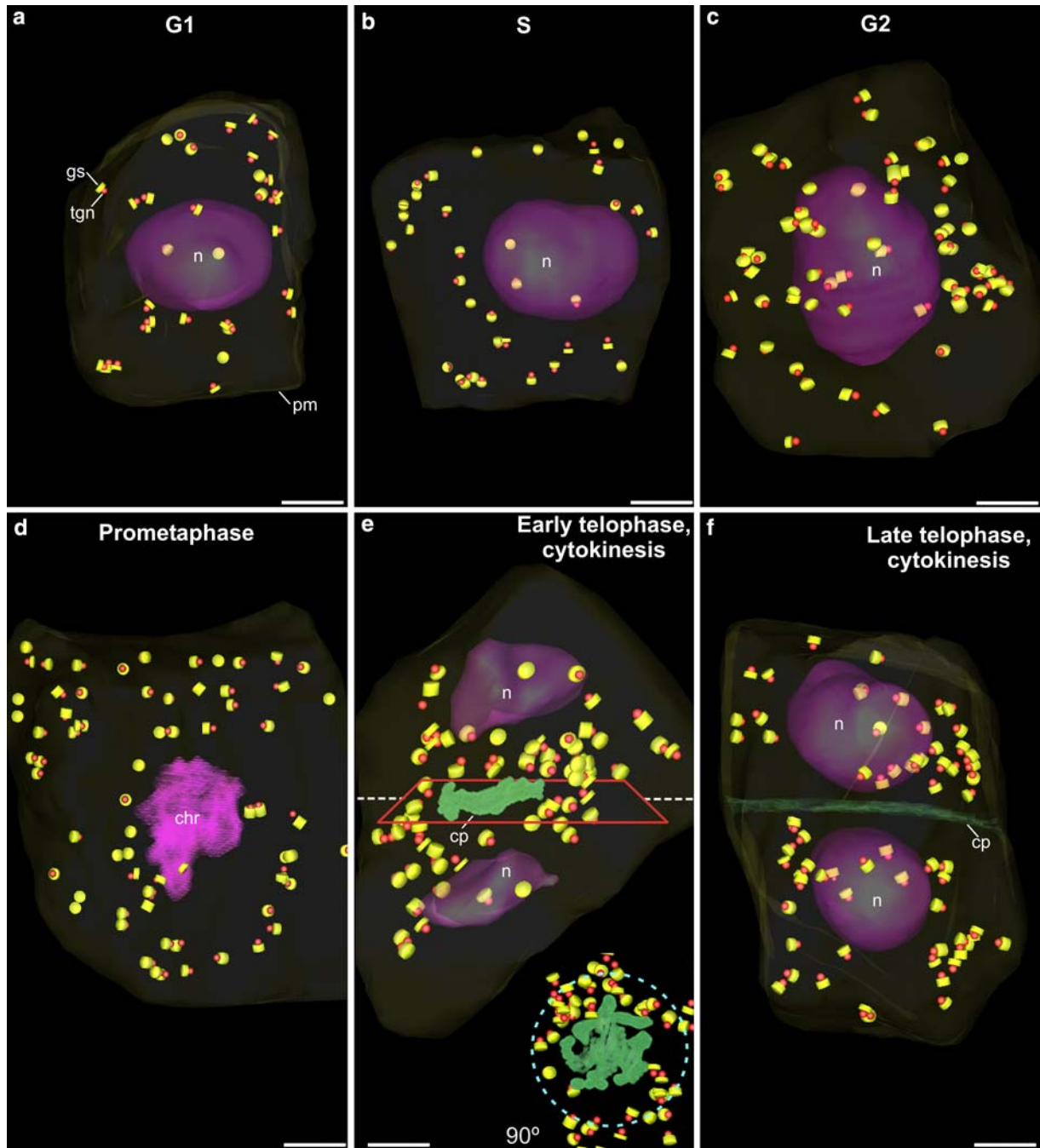


Fig. 3 Three-dimensional distribution of Golgi stacks (gs, yellow cylinders) and their associated trans-Golgi network (tgn, red spheres) through the cell cycle. **(a)** G1 **(b)** S **(c)** G2 **(d)** mitotic prometaphase **(e)** early telophase, solid phragmoplast stage of cytokinesis. The red box in **(e)** represents the midplane of the cell. Inset shows a 90°-tilted view evidencing the belt disposition of the Golgi stacks around the cell plate. **(f)** Late telophase, ring phragmoplast stage of cytokinesis. chr: chromatin; cp: cell plate; n: nucleus; pm: plasma membrane. Bars: 1 μm

stacks or TGN cisternae. It has also been reported (Samuels et al. 1995; Seguí-Simarro et al. 2004) that significant numbers of CCVs bud from maturing cell plates during the ring phragmoplast stage of cytokinesis (Fig. 2b, c), and MVBs also appear in the vicinity of such cell plates (Fig. 2b, 4f). Due to the availability of an electron tomographic database of dividing cells (Seguí-Simarro et al. 2004), we have

been able to carry out a quantitative analysis of cell plate-associated CCV formation in such cells (Fig. 5b) and correlate the findings with our serial section analysis data on MVBs (Fig. 5a). As an internal reference, we have also calculated the density of CCVs of randomly chosen central regions of mitotic metaphase cells (Fig. 5a, b). The data demonstrate that when compared to the metaphase cells, the number of cell

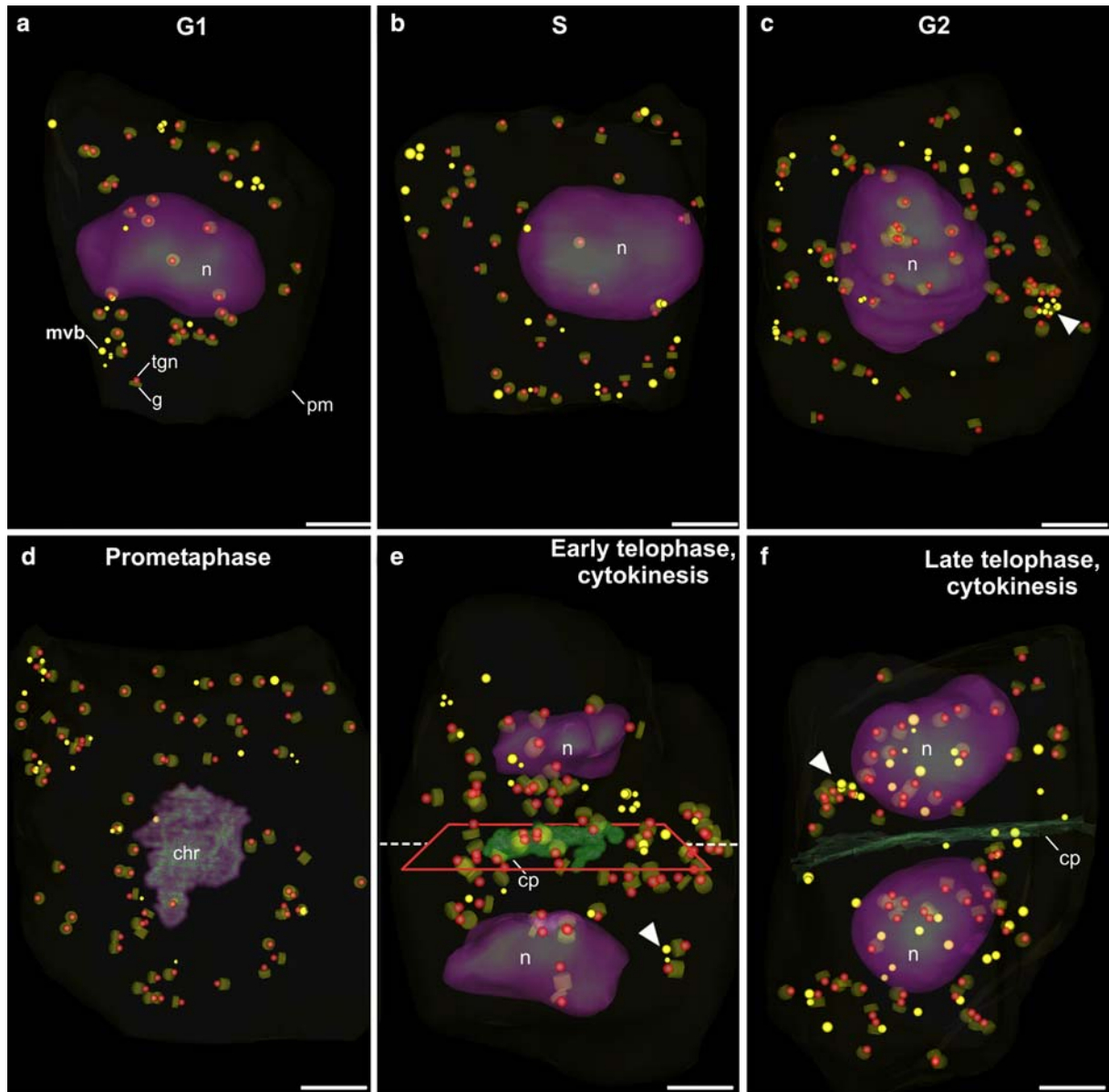


Fig. 4 Three-dimensional distribution of the multivesicular bodies (mvb, yellow spheres), with respect to Golgi stacks (g) and trans-Golgi networks (tgn) through the cell cycle. **(a)** G1 **(b)** S **(c)** G2 **(d)** mitotic prometaphase **(e)** early telophase, solid phragmoplast stage of cytokinesis. **(f)** late telophase, ring phragmoplast stage of cytokinesis. Arrowheads point to examples of multivesicular body clusters associated to trans-Golgi networks. The red box in (e) represents the midplane of the cell. chr: chromatin; cp: cell plate; n: nucleus; pm: plasma membrane. Bars: 1 μ m

plate-associated CCVs increases twofold during the solid phragmoplast stage, and fourfold during the ring phragmoplast stage of cytokinesis (Fig. 5b). These increases in CCVs are paralleled by major increases in total MVBs volume during the same cytokinetic stages (Fig. 5a).

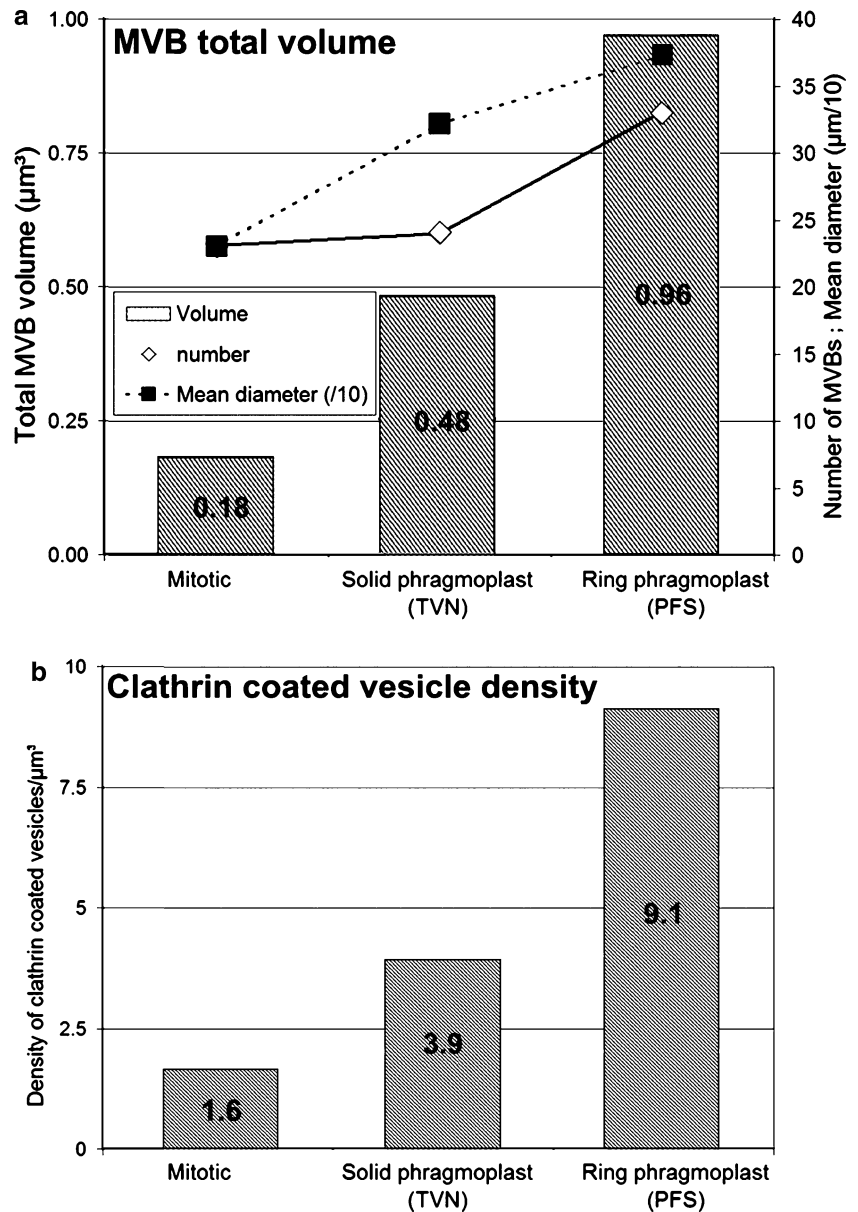
The vacuoles of apical meristem cells undergo cell cycle-dependent changes in shape, volume and distribution

Plant multivesicular bodies are involved in the endocytic pathway to the lytic vacuoles, as prevacuolar

compartments (Tse et al. 2004). For this reason, we have mapped the changes in vacuolar organization during the cell cycle to determine if any identifiable relationship between MVBs and vacuoles can be discerned.

In the reconstructed meristem cells, the vacuoles occupied a significant percentage of the cell volume, but never exceeding 14%. However, as documented in Fig. 6, the shape and organization of the vacuoles differ between each of the six stages of the cell cycle. During G1 to S, the vacuole system appears as an interconnected system of globular vacuoles of variable size (Fig. 6a, b), with both narrow and wide connecting

Fig. 5 (a) Changes in total volume (solid bars, left scale), number and mean diameter of multivesicular bodies (solid and dotted lines, respectively, right scale) during mitotic metaphase and the two main stages of cytokinesis, the solid and ring phragmoplast stages. **(b)** Density of clathrin-coated vesicles at metaphase (mitosis), and the solid and ring phragmoplast stages of cytokinesis



tubular domains. As the cell progresses towards mitosis during the G2 phase, the principal, tubular vacuole assumes a bilobed configuration foreshadowing the upcoming cytokinetic events (Fig. 6c). Simultaneously, the large vacuole appears to give rise to smaller ones through a budding-like process (Fig. 6c, arrowheads). By prometaphase, the vacuolar system assumes again a fragmented configuration consisting of few large vacuoles and numerous smaller ones (Fig. 6d). However, unlike the rounded vacuoles in G1, many of the larger prometaphase vacuoles possess short, tubular extensions. The most dramatic configurational changes of the vacuole system are observed during early telophase (Fig. 6e), when most of the vacuolar elements become sausage-like tubular structures. In addition to these shape changes, the early telophase-cytokinesis vacuolar

system undergoes a major reduction ($\sim 50\%$) in surface area, and an even greater reduction in volume ($\sim 80\%$; Fig. 7). By late telophase, but prior to the completion of the new cell wall, each daughter cell contains about half of the mostly tubular vacuolar system, which appears to wrap itself around the two reforming nuclei and extend along the cell plate (Fig. 6f). During this period, the surface area of the vacuolar system also returns to nearly the same maximal surface area as during prometaphase, while the volume doubles (Fig. 7a, b). We checked the validity of the volumetric data observed in the reconstructed cells, by estimating the fraction of cell volume occupied by vacuoles (see Materials and methods) in micrographs of randomly chosen cells at the six considered cell cycle stages (data not shown). This ratio of vacuolar vs cell volume clo-

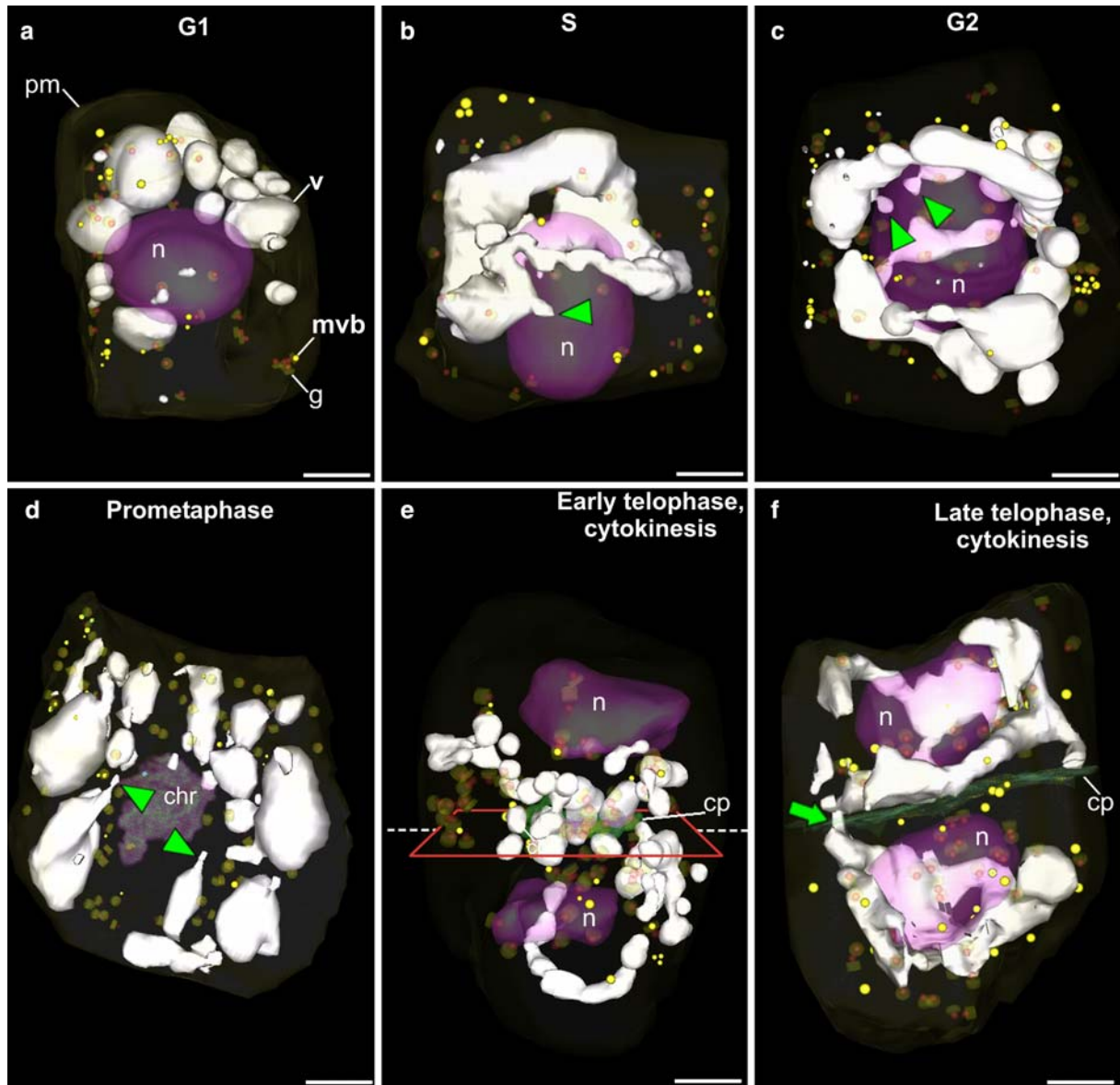


Fig. 6 Three-dimensional distribution of the vacuolar system (v, white shapes), through the cell cycle. **(a)** G1 **(b)** S **(c)** G2 **(d)** mitotic prometaphase. Note the incipient fragmentation of the vacuolar network. **(e)** Early telophase, solid phragmoplast stage of cytokinesis. Vacuoles reduce their volume, tubulate and concentrate around the cell plate (cp). **(f)** Late telophase, ring phragmoplast stage of cytokinesis. The arrow points to a vacuolar tubule, trapped by the cell plate, that connects the vacuolar network of the future daughter cells. Arrowheads point to examples of vacuolar fusion/fission events. The red box in (e) represents the midplane of the cell. chr: chromatin; g: Golgi stack; mvb: multivesicular body; n: nucleus; pm: plasma membrane. Bars: 1 μm

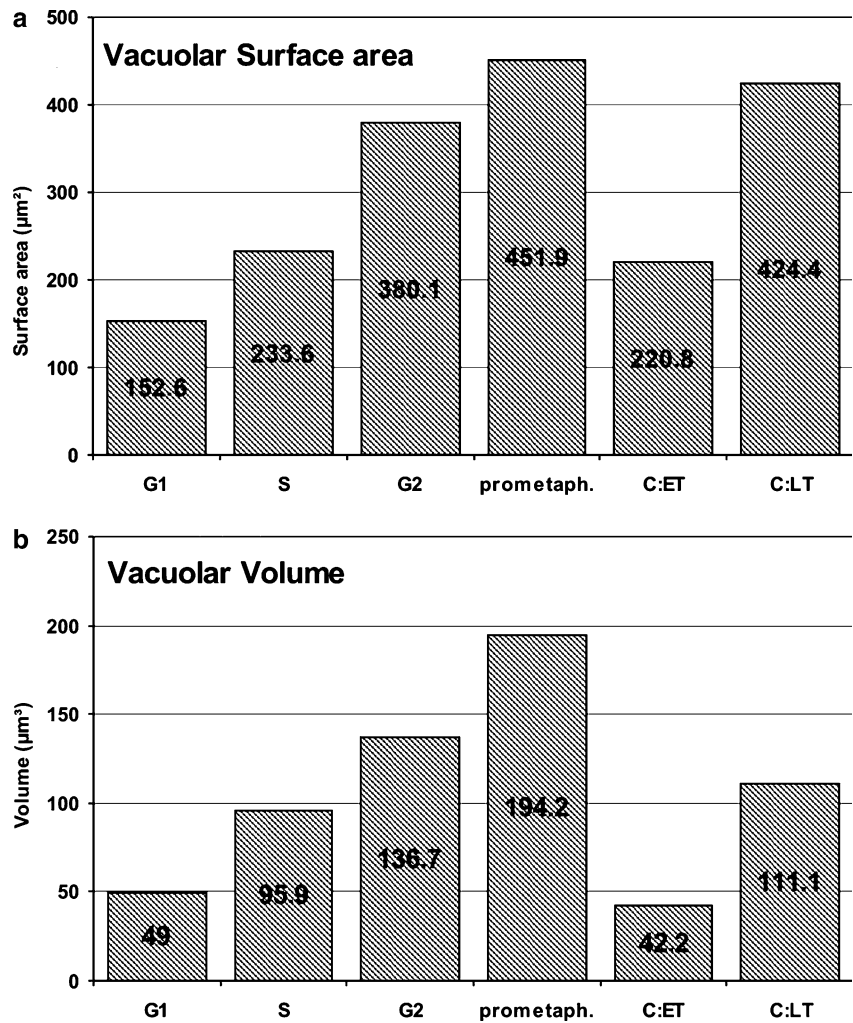
sely paralleled that of Fig. 7, confirming the observed reduction in vacuolar volume by early telophase, and proving the validity of the information provided by 3D reconstructed cells.

Multivesicular bodies were frequently observed in close proximity of large and small vacuoles, including the budding profiles (Fig. 6a–f). However, we could not detect any preferred spatial relationship between the two types of organelles. Multivesicular bodies were seen both close to and far away from vacuoles, and the changes in vacuole structure were not paralleled by distinct redistributions of MVBs (Fig. 6a–f).

Discussion

In this study we have characterized the cell cycle-dependent changes in morphology, size, number, and distribution of organelles that contribute either directly (Golgi stacks, CCVs) or indirectly (MVBs, vacuoles) to the processes of cell plate assembly and maturation. The findings both confirm some of the known attributes of these organelles in cytokinesis as well as open up new perspectives on the cellular events associated with cell division.

Fig. 7 Quantitative analysis of the changes in vacuolar surface area (a) and volume (b) during the cell cycle. Note the dramatic reduction in surface area and volume during cytokinesis at early telophase (C:ET), and the recovery at late telophase (C:LT)



Doubling of Golgi stacks occurs during the G2 stage of the cell cycle and before mitosis

Cytokinesis in plants depends on products of the Golgi apparatus. Thus, the Golgi-derived cell plate forming vesicles contribute both membrane and cell wall matrix molecules to the forming cell plate (Staehein and Moore 1995). Furthermore, because cell plate assembly is a very fast process (Ueda et al. 2003), it is of interest to know when the Golgi stacks duplicate during the cell cycle and how they become organized during cell plate assembly.

The literature on when plant Golgi double in number during the cell cycle is somewhat controversial, and is not clear to what extent this timing reflects differences in cell and plant types, or whether the differences relate to the use of different analytical protocols. The current study shows unambiguously that in *A. thaliana* apical meristem cells, the number of Golgi stacks doubles during the G2 phase of the cell cycle. This finding is based on two independent types of analyses, stereology of randomly sectioned cells, and reconstructions of serially sectioned whole cells (Table 1, Fig. 3). Doubling of the number of Golgi stacks during G2 makes func-

tional sense in apical meristem cells, both because the probability of a roughly equal distribution of Golgi stacks between the two daughter cells through a random distribution process increases with the number of Golgi units involved, and because of the formation of a cell plate within a very short period of time requires a high rate of secretory vesicle production by both daughter cells.

The contradictory reports of Golgi doubling occurring during mitosis in onion root meristem cells (Garcia-Herdugo et al. 1988), during cytokinesis in synchronized, cultured cells of *C. roseus* (Hirose and Komamine 1989), or over a broad window of time, not necessarily linked to mitosis or cytokinesis in cultured tobacco BY-2 cells (Nebenführ et al. 2000), may be due, in part to the different experimental systems studied. For example, in the large, highly vacuolated tobacco BY-2 cells, the amount of interphase cell wall synthesis required per unit cytosol is much greater than in the small *Arabidopsis* meristem cells, and therefore more new Golgi stacks might be expected to occur as the cells enlarge during interphase. However, some of the results of the earlier studies may have also been

Table 1 Numerical analysis of Golgi stacks during the cell cycle: number per cell, segregation between daughter cells and stack orientation

		Golgi stacks				
		Number of stacks / cell		Segregation into daughter cells	TGN orientation	
		Counted	Mean		facing center	facing PM
Interphase G1	G1	34	35	–	47%	53%
	S	36	–	–	47%	53%
	Estimated (stereology, 29 cells)	–	36	–	–	–
Interphase G2		66	–	–	47%	53%
Dividing	Prometaphase	69	67	–	60%	40%
	CK – TVN	65	–	29/36	54%	46%
	CK – PFS	68	–	31/37	43%	57%
	Estimated (stereology, 41 cells)	–	76	–	–	–

affected by the use of non-optimal specimen preparation methods such chemical fixation and dehydration techniques, which do not reliably preserve the dimensions of cytoplasmic organelles. Because stereological studies provide quantitative insights into the structural parameters of cells, any changes in cell dimensions can significantly affect the results of such studies. Furthermore, it should be noted that both in the onion meristem (Garcia-Herdugo et al. 1988) and in the *C. roseus* (Hirose and Komamine 1989) study, the reported Golgi doubling period was not measured or observed directly, but inferred from indirect structural parameters. Accordingly, neither of these studies provide any actual numbers of Golgi stacks per cell during the different stages of the cell cycle. This contrasts with the current study, which shows that interphase shoot apical meristem cells of *A. thaliana* possess ~35 Golgi stacks, and that the number of stacks doubles during the G2 phase of the cell cycle. Plant and algal Golgi stacks appear to multiply by division (Craig and Staehelin 1988; Hirose and Komamine 1989; Ueda 1997), but the exact mechanism is yet to be elucidated.

Most multivesicular bodies are located adjacent to clathrin-coated vesicle-producing membrane systems, the TGN and maturing cell plates

The MVBs of *A. thaliana* apical meristem cells modeled in this study vary in size from 200 to 400 nm, which is similar to the size range of multivesicular bodies in cryofixed tobacco BY-2 cells (200–500 nm; Tse et al. 2004), but smaller than reported in other studies (0.3 to several microns; Robinson et al. 1998). In part, the smaller size may be due to the use of cryofixation and freeze-substitution specimen preparation techniques, which reduces the swelling artifacts observed in chemically fixed and dehydrated specimens. However, cell- and tissue-specific differences in MVB size are likely to exist.

The finding that a majority of the MVBs are located in the vicinity of Golgi–TGN units is consistent with

their role as prevacuolar compartments that participate in both the secretory and the endocytic pathways (Tse et al. 2004). In both animal and yeast cells, the delivery of membrane and cargo molecules to MVBs involves CCVs (Ghosh and Kornfeld 2003). Similarly, plant cells employ CCVs in the trafficking of products to both lytic and storage vacuoles (Tse et al. 2004). Thus, the physical proximity of TGN and MVBs in meristem cells is a structural reflection of the underlying metabolic relationship between the two membrane compartments. The functional relationship between Golgi and MVBs in plants first emerged from the studies of the localization of prevacuolar compartment marker proteins such as BP-80/AtELP and AtSYP21 in Golgi cisternae of both *Pisum sativum* and *A. thaliana* cells (Sanderfoot et al. 1998; Hinz et al. 1999). Recently, it has been shown that in *Arabidopsis* protoplasts, a GFP:EDB (endosome-binding domain of the human Early Endosome Antigen 1, EEA1) fusion protein is primarily targeted to the TGN, and then transported to the prevacuolar compartment (Kim et al. 2001). The physical proximity between MVBs and Golgi stacks has also been noted in tobacco BY-2 cells containing both GFP- and YFP-Golgi and multivesicular body marker proteins (Tse et al. 2004), as well as in white spruce protoplasts incorporating cationized ferritin (Galway et al. 1993).

The association of MVBs with maturing cell plates has been reported previously (Samuels et al. 1995; Otegui et al. 2001; Seguí-Simarro et al. 2004). The new insights from this study pertain to the correlation between the increase in the number of cell plate-associated clathrin-coated buds and vesicles during the later stages of cytokinesis and the parallel increases in both the total number of MVBs and the volume of the average MVB (Fig. 5). The marked increase in number and size of the MVBs during periods of high CCV production reflects not only on the magnitude of cell plate membrane recycling during cell plate formation, but also suggests that the CCVs that bud from the cell plate membrane are delivered to MVBs for recycling and/or degradation.

A putative role for the vacuolar system in early cytokinetic events?

We have shown that the vacuole system of proliferating meristem cells undergoes major structural changes as the cells progress through the cell cycle. Most notably, at the onset of mitosis, the network fragments into many independent vacuoles of variable size (Fig. 6d). A similar fragmentation of the vacuolar system during mitosis has been observed in horseradish root meristems cells (Marty 1999). In BY-2 cells, branched tubular strands of vacuolar membrane extend across the phragmoplast and the expanding cell plate, connecting both vacuolar domains (Kutsuna and Hasezawa 2002; Kutsuna et al. 2003). Vacuole fragmentation and presence of vacuolar tubules at the cell equator seems to be a common feature of mitosis and early cytokinesis in cell types as different as horseradish root meristem cells, cultured BY-2 cells and *Arabidopsis* shoot meristem cells. This structural rearrangement may reflect an involvement of the vacuolar system in the early stages of cytokinesis, in particular, during the establishment of the cytokinetic machinery.

As the cell progresses from mitosis to cytokinesis (Fig. 6d, e), the surface area of the fragmented vacuoles is reduced by half, and their volume decreases by ~80% (Fig. 7). The mechanism of this reduction in vacuole membrane surface area remains unclear. The presence of small, narrow tubular extensions on the larger vacuoles in the prometaphase cell shown in Fig. 6d, suggests that this process may involve the budding of vesicles or even of short, narrow tubules, which might be difficult to positively identify in thin section electron micrographs. The net result of these changes in vacuole surface area and volume is a transient increase in the volume of the cytosol, which might be needed to accommodate the volume of the phragmoplast microtubule array and associated cell plate-forming structures. The rapid recovery of the vacuole surface area during late cytokinesis (within 15–20 min of the rapid reduction in vacuole surface area during mitosis; Fig. 7a; Ueda et al., 2003), suggests that the vacuole membrane removed during mitosis might be stored transiently in a pool of yet-to-be identified membrane vesicles or tubules that can quickly re-expand the vacuole system. An interesting topic of future research will be the elucidation of the mechanism of rapid vacuole membrane shrinkage and re-growth during the mitotic and cytokinetic stages of the cell cycle of *A. thaliana* apical meristem cells.

Acknowledgements We thank Mr. Ricardo Mantilla (CIRES, University of Colorado, Boulder, CO, USA) and Prof. Jaime Renau-Piqueras (Centro de Investigación Hospital “La Fe”, Valencia, Spain) for their mathematical advice, and Mrs. Erin White (MCDB, University of Colorado, Boulder, CO, USA) for her valuable help. Many thanks are also due to David Mastronarde and the rest of members of the Boulder Laboratory for 3-Dimensional Electron Microscopy of Cells (MCDB, University of Colorado, Boulder, CO, USA, Grant RR00592). This work was supported by National Institute of Health Grant GM 61306 to L.A.S.

References

- Baskin TI, Cande WZ (1990) The structure and function of the mitotic spindle in flowering plants. *Annu Rev Plant Physiol Plant Mol Biol* 41:277–315
- Batoko H, Zheng HQ, Hawes C, Moore I (2000) A Rab1 GTPase is required for transport between the endoplasmic reticulum and Golgi apparatus and for normal Golgi movement in plants. *Plant Cell* 12:2201–2217
- Craig S, Staehelin LA (1988) High-pressure freezing of intact plant tissues - Evaluation and characterization of novel features of the endoplasmic reticulum and associated membrane systems. *Eur J Cell Biol* 46:80–93
- Delesse MA (1847) Procédé mécanique pour déterminer la composition des roches. *CR Acad Sci Paris* 25:544–545
- Galway ME, Rennie PJ, Fowke LC (1993) Ultrastructure of the endocytotic pathway in glutaraldehyde-fixed and high-pressure frozen freeze-substituted protoplasts of white spruce (*Picea glauca*). *J Cell Sci* 106:847–858
- García-Herdugo G, González-Reyes F, Gracia-Navarro F, Navas P (1988) Growth kinetics of the Golgi apparatus during the cell cycle in onion root meristems. *Planta* 175:305–312
- Ghosh P, Kornfeld S (2003) AP-1 binding to sorting signals and release from clathrin-coated vesicles is regulated by phosphorylation. *J Cell Biol* 160:699–708
- Hahn GJ, Shapiro SS (1967) *Statistical models in engineering*. John Wiley, New York
- Hawes C, Brandizzi F (2004) The Golgi apparatus - still causing problems after all these years! *Cell Mol Life Sci* 61:131–132
- Hepler PK, Wolniak SM (1984) Membranes in the mitotic apparatus - Their structure and function. *Int Rev Cytol* 90:169–238
- Herman EM, Larkins BA (1999) Protein storage bodies and vacuoles. *Plant Cell* 11:601–613
- Hinz G, Hillmer S, Baumer M, Hohl I (1999) Vacuolar storage proteins and the putative vacuolar sorting receptor BP-80 exit the Golgi apparatus of developing pea cotyledons in different transport vesicles. *Plant Cell* 11:1509–1524
- Hirose S, Komamine A (1989) Changes in ultrastructure of Golgi apparatus during the cell cycle in a synchronous culture of *Catharanthus roseus*. *New Phytol* 111:599–605
- Jürgens G (2004) Membrane trafficking in plants. *Ann Rev Cell Dev Biol* 20: 481–504
- Kim DH, Eu YJ, Yoo CM, Kim YW, Pih KT, Jin JB, Kim SJ, Stenmark H, Hwang I (2001) Trafficking of phosphatidylinositol 3-phosphate from the trans-Golgi network to the lumen of the central vacuole in plant cells. *Plant Cell* 13:287–301
- Kremer JR, Mastronarde DN, McIntosh JR (1996) Computer visualization of three-dimensional image data using IMOD. *J Struct Biol* 116:71–76
- Kutsuna N, Hasezawa S (2002) Dynamic organization of vacuolar and microtubule structures during cell cycle progression in synchronized tobacco BY-2 cells. *Plant Cell Physiol* 43:965–973
- Kutsuna N, Kumagai F, Sato MH, Hasezawa S (2003) Three-dimensional reconstruction of tubular structure of vacuolar membrane throughout mitosis in living tobacco cells. *Plant Cell Physiol* 44:1045–1054
- Marcote MJ, Gu F, Gruenberg J, Aniento F (2000) Membrane transport in the endocytic pathway: animal versus plant cells. *Protoplasma* 210:123–132
- Marty F (1999) Plant vacuoles. *Plant Cell* 11:587–599
- Mastronarde DN (1997) Dual-axis tomography: An approach with alignment methods that preserve resolution. *J Struct Biol* 120:343–352
- Mogelsvang S, Gomez-Ospina N, Soderholm J, Glick BS, Staehelin LA (2003) Tomographic evidence for continuous turnover of Golgi cisternae in *Pichia pastoris*. *Mol Biol Cell* 14:2277–2291
- Mollenhauer HH, Morre DJ, Griffing LR (1991) Post-Golgi apparatus structures and membrane removal in plants. *Protoplasma* 162:55–60
- Nebenführ A, Staehelin LA (2001) Mobile factories: Golgi dynamics in plant cells. *Trends Plant Sci* 6:160–167

- Nebenführ A, Gallagher LA, Dunahay TG, Frohlick JA, Mazurkiewicz AM, Meehl JB, Staehelin LA (1999) Stop-and-go movements of plant Golgi stacks are mediated by the actomyosin system. *Plant Physiol* 121:1127–1142
- Nebenführ A, Frohlick JA, Staehelin LA (2000) Redistribution of Golgi stacks and other organelles during mitosis and cytokinesis in plant cells. *Plant Physiol* 124:135–151
- Otegui MS, Mastrorarde DN, Kang BH, Bednarek SY, Staehelin LA (2001) Three-dimensional analysis of syncytial-type cell plates during endosperm cellularization visualized by high resolution electron tomography. *Plant Cell* 13:2033–2051
- de Paz P (1998) Estereología. In: Renau-Piqueras J, Megías L (eds) *Manual de técnicas de microscopía electrónica (M.E.T.). Aplicaciones biológicas*. Universidad de Granada, Granada, Spain, pp 439–473
- Risueño MC, Medina FJ (1986) The nucleolar structure in plant cells. *Servicio Editorial de la Universidad del País Vasco, Leioa, Vizcaya, España*
- Risueño MC, Testillano PS, Sánchez-Pina MA (1988) Variations of nucleolar ultrastructure in relation to transcriptional activity during G1, S, G2 of microspore interphase. In: Cresti M, Gori P, Paccini E (eds) *Sexual Plant Reproduction*. Springer-Verlag, Berlin, Heidelberg, pp 9–14
- Robinson DG, Baumer M, Hinz G, Hohl I (1998) Vesicle transfer of storage proteins to the vacuole: The role of the Golgi apparatus and multivesicular bodies. *J Plant Physiol* 152:659–667
- Samuels AL, Giddings TH, Jr., Staehelin LA (1995) Cytokinesis in tobacco BY-2 and root tip cells: a new model of cell plate formation in higher plants. *J Cell Biol* 130:1345–1357
- Sanderfoot AA, Ahmed SU, Marty-Mazars D, Rapoport I, Kirchhausen T, Marty F, Raikhel NV (1998) A putative vacuolar cargo receptor partially colocalizes with AtPEP12p on a prevacuolar compartment in Arabidopsis roots. *Proc Natl Acad Sci USA* 95:9920–9925
- Seguí-Simarro JM (2001) Embryogenesis induction in pollen: Cellular characterization and expression of stress proteins. PhD doctoral thesis. Complutense University of Madrid, Madrid
- Seguí-Simarro JM, Austin JR, White EA, Staehelin LA (2004) Electron tomographic analysis of somatic cell plate formation in meristematic cells of Arabidopsis preserved by high-pressure freezing. *Plant Cell* 16:836–856
- Staehelin LA, Moore I (1995) The plant Golgi apparatus - Structure, functional organization and trafficking mechanisms. *Annu Rev Plant Physiol Plant Mol Biol* 46:261–288
- Staehelin LA, Newcomb EH (2000) Membrane structure and membranous organelles. In: Buchanan B, Gruissem W, Jones R (eds) *Biochemistry and molecular biology of plants*. American Society of Plant Physiologists, pp 1–50
- Staehelin LA, Giddings TH, Jr., Kiss JZ, Sack FD (1990) Macromolecular differentiation of Golgi stacks in root tips of Arabidopsis and Nicotiana seedlings as visualized in high pressure frozen and freeze-substituted samples. *Protoplasma* 157:75–91
- Steer MW (1981) *Understanding cell structure*. Cambridge University Press, Cambridge
- Tanchak MA, Fowke LC (1987) The morphology of multivesicular bodies in soybean protoplasts and their role in endocytosis. *Protoplasma* 138:173–182
- Tse YC, Mo BX, Hillmer S, Zhao M, Lo SW, Robinson DG, Jiang LW (2004) Identification of multivesicular bodies as prevacuolar compartments in Nicotiana tabacum BY-2 cells. *Plant Cell* 16:672–693
- Ueda K (1997) The synchronous division of dictyosomes at the premitotic stage. *Ann Bot* 80:29–33
- Ueda K, Sakaguchi S, Kumagai F, Hasezawa S, Quader H, Kristen U (2003) Development and disintegration of phragmoplasts in living cultured cells of a GFP::TUA6 transgenic Arabidopsis thaliana plant. *Protoplasma* 220:111–118
- Williams M (1977) Stereological techniques. In: Glauert AM (ed) *Practical methods in electron microscopy*. North Holland/American Elsevier, Amsterdam, pp 5–84